 CMES, vol.85, no.2, pp.129-155, 2012

Vibration Analysis of Curved Shell using B-spline Wavelet on the Interval (BSWI) Finite Elements Method and General Shell Theory

Zhibo Yang[1], Xuefeng Chen[2], Bing Li[1], Zhengjia He[1] and Huihui Miao[1]

Abstract: The implementation of the B-spline Wavelet on the Interval (BSWI) for curved shell elements with rectangular planform is presented in this paper. By aid of the general shell theory, cylinder shells, doubly-curved shallow shells and hyperbolic paraboloidal shells BSWI elements are formulated. Instead of traditional polynomial interpolation, scaling functions at certain scale have been adopted to form the shape functions and construct wavelet-based elements. Because of the good character of BSWI scaling functions, the BSWI curved shell elements combine the accuracy of wavelet-based elements approximation and the character of B-spline functions for structural analysis. Different from the flat shell elements, the curved shell elements obtain a better geometrical fitting property in idealizing the practical curved structures. This paper focuses on the dynamic analysis of shell. The study covers wide combinations of boundaries such as cantilever, simply supported and clamped boundary. Numerical results have been established to validate the efficiency and accuracy of the presented elements through comparison with published data from the open literature and some commercial finite element method software.

Keywords: B-spline wavelet on the interval, wavelet-based element, curved shell, vibration analysis.

1 Introduction

From the view of geometry, shells are depicted as the three dimensional solids confined by two general surfaces. The scale between the two general surfaces is small compared with the other scales of shell. From the view of the mechanics, the shell can be seen as a degraded model of the three dimensional solid whose displacement of a certain dimension is uniform through the normal direction [Chao and Reddy

[1] The State Key Laboratory for Manufacturing Systems Engineering.
[2] Corresponding author. School of Mechanical Engineering, Xi'an Jiaotong University, P.R. China.

(1984)]. Owing to its practical importance and the computational efficiency, the study of shell structures has long been an extensive topic for the past decades in the applications of aerospace, civil and mechanical engineering [Atluri (1985); Voyiadjis and Shi (1991); Iura and Atluri (1992); Bathe, Iosilevich, Chapelle (2000)].

Considering the coupling between extensional and bending stiffness, the theory of curved shells is more complex than that of plates. Different from plates, where there is a widely accepted plate theory, the theoretical study of shells is still an open proposition. Many kinds of theories can be used for modeling shells with an acceptable accuracy. Under the revolutionary shell theory [Artioli, Gould, Viola (2005);], shells are simplified as one-dimension structures similar to beam. The Donnell-Mushtari theory [Zhang and Atluri (1986); Qatu (1992, 1999); Qatu and Asadi (2012)], which is also a simplification of general theory, is more suitable for shallow shells. It is evident that these simplifications or assumptions are only appropriate for some special cases of shells, thus we will use the basic general shell theory for element formulation in this paper [Huang, Shenoy and Atluri (1994); Tornabene, Viola and Inman (2009); Tornabene (2011)]. The general shell theory is the theoretical basis of other theories, and it will approach to these theories when some parameters trend to assumptions.

Unlike the flat shells, curved shells are based on shell hypothesis and formulated by the general shell theory directly. The coupling between in-plane and out-plane displacements are considered in the derivation process. Thus, it can fit the structures such as arches well. However, flat shells are only formulated by combining a membrane element for plane elasticity and a bending element for plate theory simply [Nguyen-Xuan, Rabczuk, Bordas and Debongnie (2008); Nguyen-Xuan, Bordas, Nguyen-Thanh and Rabczuk (2008)], moreover, an additional drilling degree must be contained in analysis, which is not claimed to construct the theoretical foundation and will cause a considerable consumption of memory space [Zienkiewicz and Taylor (2000)]. To idealize the curved structures, a spatial transform matrix must be used, which also leads in deviations in geometry and additional consumptions in computing. The visual differences between the formulation of flat and curved shell elements are presented in Fig. 1.

For decades, numerous papers concerned the continuum or discrete analyses of curved shells that have been published mainly based on Kirchhoff-Love assumption (Thin shell theory) and Reissner-Mindlin assumption (First-order theory). It has been known that the assumptions in Kirchhoff-Love theory will lose their validity with the increase of the panel thickness [Liew and Lim (1995a)]. However, shells based on Reissner-Mindlin assumption have extensive engineering applications range and adaptability for the increases of the panel thickness. Until now, research work related to this field has been intensively investigated. A series of early

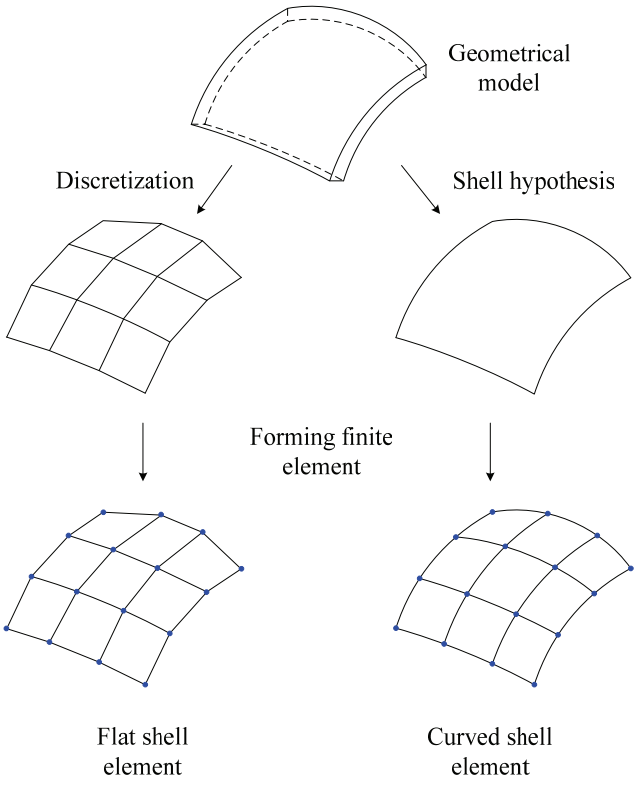

Figure 1: Illustration of the formulations for the flat shell element and curved shell element

studies related to this subject were given by Cowper, Lindberg and Olson [Cowper, Lindberg and Olson (1970); Olson and Lindberg (1971)], in which some static problems and experiments involving transverse loading were analyzed. Apart from these work, Leissa and Kadi [Leissa and Kadi (1971)] investigated the curvature effects on shallow shell vibrations. In the 1980's, more interests in this problem were presented. Using the Ritz method with algebraic polynomial trial functions, the group of Leissa studied the vibrations of cantilevered doubly-curved shallow shells with rectangular planform systematically [Leissa, Lee and Wang (1983)]. Reddy and his co-workers studied the laminated shells using moderately thick theory and three dimension finite element method [Reddy (1984); Chao and Reddy (1984)]. In addition, another combined boundary/interior element method proposed by Zhang and Atluri should be also mentioned. Based on this approach, they studied the static stress, free-vibration and transient response of shallow shells [Zhang and Atluri

(1986)]. In the 1990's, based on Ritz method and its improvements, Lim and Liew together with their colleges made a number of remarkable investigations of shell structures: The pb-2 Ritz energy based approach, along with deflections assumed in the form of a product of complete two-dimensional orthogonal polynomials and a basic function, is employed to model the vibratory characteristic of shells [Liew and Lim (1995b, 1996)]; Combined with the Ritz method, a higher order shear deformation theory is proposed to analyse the effects of various shell geometries and boundary conditions on the vibration responses [Lim and Liew (1995)]; The vibratory characteristics of shells subjected to different boundary conditions were obtained via a three-dimensional displacement-based energy formulation employed the p-Ritz method [Liew, Peng and Ng (2002)]; And the analysis of thick shallow shells vibrating at high modes was given by using the discrete singular convolution (DSC)-Ritz method on Mindlin plates and shells with various edge supports [Lim, Li and Wei (2005)]. Apart from their work, Bathe investigated the mixed interpolation of tensorial components (MITC) shell element and the convergence behavior of common shell element with his group [Eucalemi and Bathe (1993); Bathe and Lee (1997, 2011); Bathe, Iosilevich and Chapelle (2000)]. Kulikov and Plotnikova proposed a geometrically exact four-node solid-shell element based on the first-order theory for analyses of homogeneous and multilayered composite shells undergoing finite rotations [Kulikov and Plotnikova (2002, 2008, 2011)]. Furthermore, the variable thickness shell was studied by Kang and Leissa using Ritz method [Kang and Leissa (2000)]. By means of the third-order shear deformation theories and the strain-displacement relations of shell, Lee and Reddy solved the problem of vibration suppression of laminated shell structures [Lee and Reddy (2004)]. More available literatures on shells can be found in some comprehensive reviews of the groups of Qatu, Liew and Reddy [Qatu (1992); Liew, Lim and Kitipornchai (1997); Reddy and Arciniega (2004)].

High performance computing is an essential issue for some numerical simulation problems, including the vibration analysis of shells. Some new numerical methods have been developed in recent years, such as meshless local Petrov-Galerkin (MLPG) method [Atluri and Zhu (1998); Atluri, Kim and Cho (1999)], the generalized differential quadrature (GDQ) method [Viola and Tornabene (2009)], the H-adaptive local radial basis function meshless method [Kosec and Sarler (2011)], boundary element method [Sapountzakis and Mokos (2009)], and the discontinuous Galerkin method [Noels and Radovitzky (2008)] etc. The wavelet-based numerical analysis is also a new method developed in recent years. It can be viewed as a finite element method in which the approximation functions are selected as the scaling or wavelet functions, similar to those used in signal or image processing. This method is well argued by many researchers in structural analysis fields [Chen

and Wu (1995, 1996a, 1996b); Han, Ren and Huang (2005, 2006, 2007); Xiang, Long and Jiang (2010); Zhong and Xiang (2011)]. However, most of the wavelet functions used now lacking an explicit expression, which would cause numerical error when finite element solving equation is formulated [Xiang and Liang (2011), Xiang and Matsumoto et. al (2011)]. Compared with the interpolation wavelet function basis used now, B-spline wavelet on the interval (BSWI) basis has the good characteristics of compact support, smoothness and symmetry in addition to the multi-resolution analysis. Moreover, it has the explicit expression, which will not lead any trouble for differentiation and integration. Furthermore, as a type of generalized spline finite element method, BSWI element inherits the superiority of spline for structural analysis. In this paper, we will present a new BSWI curved shell element for vibration analysis. Compared with flat shell elements, a great deal of numerical complexity is involved because the vibratory field is increased to five degrees of freedom (three for the orthogonal displacement and two for the transverse rotations) and the coupling of them is considered. Nevertheless, it is highly efficient and economic because there is no geometry approximation being used in the analysis of curved structures.

The outline of this paper is as follows. In section 2, the basic equations of curved shells are given from general shell theory as the basement of the element formulation. In section 3, the short introduction of the BSWI functions are presented. A class of BSWI curved shell elements are constructed in section 4. At last, section 5 provides some numerical examples and comparisons which demonstrate accuracy and efficiency of the presented elements.

2 Basic equations of curved shells

2.1 Problem definition

Consider a common curved shell of rectangular planform with thickness h and a pair of radii of curvature at the mid-surface R_x and R_y as shown in Fig. 2. The geometry of the shell is defined in natural coordinate system XYZ, where X and Y denote the tangential of surface, and Z denotes the normal of shells. From the common model given in Fig. 2, three kinds of special curved shell are obtained by selecting the different ratio of R_x/R_y. The geometry of the circular cylinder, doubly-curved shallow shell and hyperbolic paraboloidal shell are presented in Fig. 3. Let $R_y = \infty$, so that $R_x/R_y = 0$, the model will be the circular cylinder as shown in Fig. 3(a); Let R_x/R_y equal to a positive constant, the model will be the doubly-curved shallow shell as shown in Fig. 3(b); Let R_x/R_y equal to a negative constant, the model will be the hyperbolic paraboloidal shallow shell as shown in Fig. 3(c). Some denotations in Fig. 3 are explained here: the span lengths along x-axis and y-

axis (Cartesian coordinate) are expressed as a and b; the corresponding span angles are denoted as θ_x and θ_y. For convenience, some denotations of boundaries are used: free boundary (F), simply supported boundary (S) and the clamped boundary (C).

2.2 Theoretical formulation

The present investigation is based on the first-order shear deformation theory. The relations among orthogonal deflection components u, v and w and their mid-surface orthogonal deflection components u_0, v_0, w_0, and rotations ψ_x and ψ_y are given as follows:

$$u = \left(1 + \frac{z}{R_x}\right) u_0 + z\psi_x \tag{1}$$

$$v = \left(1 + \frac{z}{R_y}\right) v_0 + z\psi_y \tag{2}$$

$$w = w_0 \tag{3}$$

The biggest difference between shell and solid is that the strain $\varepsilon_{33} = 0$ in shell analysis. Thus, consider the assumptions given in Eqs. (1a-1c) and neglect the higher order terms of strain, the strain fields under general shell theory are expressed as:

The membrane strain $\boldsymbol{\varepsilon} = \left\{\varepsilon_{11} \quad \varepsilon_{22} \quad \varepsilon_{12}\right\}^{\mathrm{T}}$:

$$\begin{cases} \varepsilon_{11} = \frac{1}{A_1}\frac{\partial u_1}{\partial s_1} + \frac{u_2}{A_1 A_2}\frac{\partial A_1}{\partial s_2} + \frac{w}{R_1} \\ \varepsilon_{22} = \frac{1}{A_2}\frac{\partial u_2}{\partial s_2} + \frac{u_1}{A_1 A_2}\frac{\partial A_2}{\partial s_1} + \frac{w}{R_2} \\ \varepsilon_{12} = \frac{A_1}{A_2}\frac{\partial}{\partial s_2}\left(\frac{u_1}{A_1}\right) + \frac{A_2}{A_1}\frac{\partial}{\partial s_1}\left(\frac{u_2}{A_2}\right) \end{cases} \tag{4}$$

The curvature strain $\boldsymbol{\kappa} = \left\{\kappa_{11} \quad \kappa_{22} \quad \kappa_{12}\right\}^{\mathrm{T}}$:

$$\begin{cases} \kappa_1 = \frac{1}{A_1}\frac{\partial \psi_x}{\partial s_1} + \frac{\psi_y}{A_1 A_2}\frac{\partial A_1}{\partial s_2} \\ \kappa_2 = \frac{1}{A_2}\frac{\partial \psi_y}{\partial s_2} + \frac{\psi_x}{A_1 A_2}\frac{\partial A_2}{\partial s_1} \\ \kappa_{12} = \frac{1}{A_1}\frac{\partial \psi_x}{\partial s_1} + \frac{\psi_y}{A_1 A_2}\frac{\partial A_1}{\partial s_2} + \frac{1}{A_2}\frac{\partial \psi_y}{\partial s_2} + \frac{\psi_x}{A_1 A_2}\frac{\partial A_2}{\partial s_1} \end{cases} \tag{5}$$

The transverse shear strain $\boldsymbol{\gamma} = \left\{\gamma_1 \quad \gamma_2\right\}^{\mathrm{T}}$:

$$\begin{cases} \gamma_1 = \frac{\partial w}{\partial s_1} - \psi_x \\ \gamma_2 = \frac{\partial w}{\partial s_2} - \psi_y \end{cases} \tag{6}$$

in which A_1 and A_2 are the Lame coefficients, s_1 and s_2 are the variables with corresponding Lame coefficients. For flat shell, $A_1 = A_2 = 1$ and $s_1 = L_x, s_2 = L_y$; for cylinder shell (Fig. 3(a)), $A_1 = R, A_2 = 1$ and $s_1 = \theta_x, s_2 = L_y$; for the doubly-curved shell and the hyperbolic paraboloidal shell, $A_1 = R_x, A_2 = R_y$ and $s_1 = \theta_x, s_2 = \theta_y$. L_x and L_y are the length on x and y directions (Fig. 3(b,c)), respectively.

Considering the transverse shear strain, the total stain energy of shells consists of three parts:

$$U = U_\varepsilon + U_\kappa + U_\gamma \tag{7}$$

in which

$$U_\varepsilon = \frac{1}{2}\iint_\Omega \boldsymbol{\varepsilon}^{\mathrm{T}}\mathbf{D}^m\boldsymbol{\varepsilon}\mathrm{d}\Omega \tag{8}$$

$$U_\kappa = \frac{1}{2}\iint_\Omega \boldsymbol{\kappa}^{\mathrm{T}}\mathbf{D}^b\boldsymbol{\kappa}\mathrm{d}\Omega \tag{9}$$

$$U_\gamma = \frac{1}{2}\iint_\Omega \boldsymbol{\gamma}^{\mathrm{T}}\mathbf{D}^t\boldsymbol{\gamma}\mathrm{d}\Omega \tag{10}$$

with

$$\mathbf{D}^m = \frac{Eh}{(1-v)^2}\begin{bmatrix} 1 & v & 0 \\ v & 1 & 0 \\ 0 & 0 & (1-v)/2 \end{bmatrix} \tag{11}$$

$$\mathbf{D}^b = \frac{Eh^3}{12(1-v)^2}\begin{bmatrix} 1 & v & 0 \\ v & 1 & 0 \\ 0 & 0 & (1-v)/2 \end{bmatrix} \tag{12}$$

$$\mathbf{D}^t = \frac{kEh}{2(1+v)}\begin{bmatrix} 1 & 0 \\ 0 & 1 \end{bmatrix} \tag{13}$$

To express briefly in the following parts, we denote the coefficient in front of the matrixes in Eq. (7) as D_0^m, D_0^b and kD_0^t, respectively. k is called shearing correction factor. The kinetic energy is:

$$\begin{aligned} T = {} & \tfrac{1}{2}\rho\int_\Omega \left[\left(\tfrac{\partial u}{\partial t}\right)^2 + \left(\tfrac{\partial v}{\partial t}\right)^2 + \left(\tfrac{\partial w}{\partial t}\right)^2\right] h\mathrm{d}\Omega \\ & + \tfrac{1}{2}\rho\int_\Omega \left[\left(\tfrac{\partial \psi_x}{\partial t}\right)^2 + \left(\tfrac{\partial \psi_y}{\partial t}\right)^2\right] \tfrac{h^3}{12}\mathrm{d}\Omega \end{aligned} \tag{14}$$

where the symbol ρ is the mass density of material and symbol t expresses time. The variational energy function is defined as the difference between the strain energy and the kinetic energy:

$$\Pi = U - T \tag{15}$$

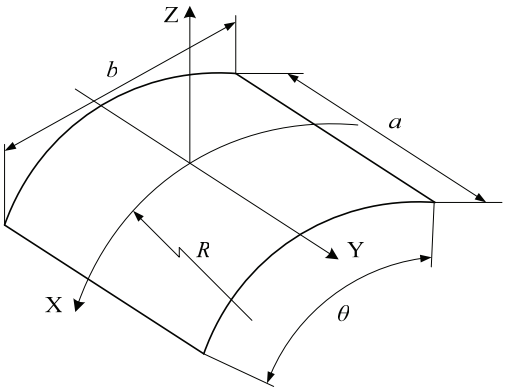

(a) The circular cylinder

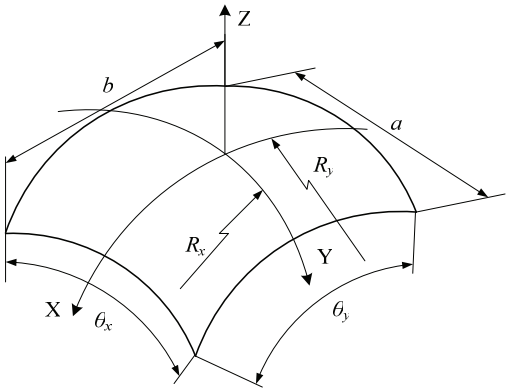

(b) The doubly-curved shell

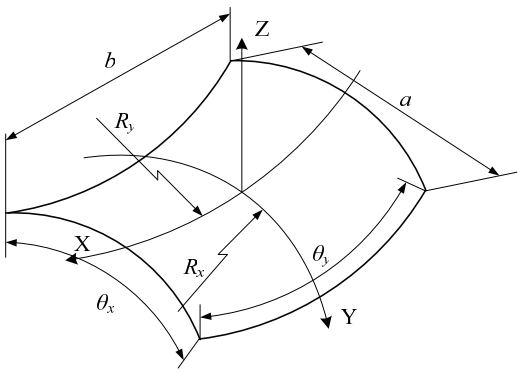

(c) The hyperbolic paraboloidal shell

Figure 2: Geometry of curved shells

3 Two-dimensional B-spline Wavelet on the Interval

The B-spline in a given simple knot sequence can be constructed by employing piecewise polynomials between the knots and joining them together at the knots. In this way, the overall smooth B-splines in C^{m-2} will be obtained if the order is assigned to m. By means of a simple linear mapping $\xi = (x-a)/(b-a)$, any one dimensional function $f(x)$ on the interval $[a, b]$ can be transferred to the interval [0, 1]. Thus, it only needs to construct the mth order B-spline function on the interval [0, 1]. As interval wavelets, B-spline on interval [0, 1] was given by Goswami, Chan and Chui [Goswami, Chan and Chui (1995)]. Since there should be at least

one inner wavelet on the interval [0, 1], the following condition must be satisfied:

$$2^j \geq 2m-1 \tag{16}$$

where j is the scale number of BSWI. According to the 0 scale mth order B-spline functions and the corresponding wavelets given by Goswami [Goswami, Chan and Chui (1995)], the j scale mth order BSWI, simply denoted as BSWIm_j, scaling functions $\varphi^j_{m,k}(\xi)$ are derived by following formulas:

$$\varphi^j_{m,k}(\xi) = \begin{cases} \varphi^l_{m,k}(2^{j-1}\xi), & k=-m+1,\ldots,-1 \text{ (0 boundary scaling functions)} \\ \varphi^l_{m,2^j-m-k}(1-2^{j-l}\xi), & k=2^j-m+1,\ldots,2^j-1 \text{ (1 boundary scaling functions)} \\ \varphi^j_{m,0}(2^{j-l}\xi-2^{-l}k), & k=0,\ldots,2^j-m \text{ (inner scaling functions)} \end{cases} \tag{17}$$

Therefore, the scaling functions on the interval [0, 1] can be written in the vector form:

$$\Phi = \left\{ \varphi^j_{m,-m+1}(\xi)\ \varphi^j_{m,-m+2}(\xi)\ldots\varphi^j_{m,2^j-1}(\xi) \right\} \tag{18}$$

where ξ belongs to interval [0, 1]. Kronecker product, which is also called tensor product, is an easy way to construct two dimensional BSWI from the one dimensional ones. The new two dimensional scaling or approximation space F_j is constructed by the Kronecker product of one dimensional approximation spaces V^1_j and $V^2_j (F_j = V^1_j \otimes V^2_j)$, and the new basement is $\Phi = \Phi_1 \otimes \Phi_2$, where subscripts 1 and 2 are used to distinguish the different variations in scaling functions as given in Eq. (12). The one dimensional and two dimensional BSWI4$_3$ scaling functions we used in this paper as the shape function for curved shell element is presented in Fig. 4.

4 Formulation of BSWI curved shell elements

Using Hamilton's principle, the following equation of motions for free vibration analysis can be derived in a short time interval $[t_1, t_2]$:

$$\delta \int_{t_1}^{t_2} \Pi \mathrm{d}t = \delta \int_{t_1}^{t_2} (U-T)\mathrm{d}t = 0 \tag{19}$$

Denote $\mathbf{d} = \left\{ u \quad v \quad w \quad \psi_x \quad \psi_y \right\}^{\mathrm{T}}$, the finite element analysis, the normal displacement, tangential displacements and rotation should be interpolated by BSWI4$_3$

scaling functions respectively following the first order shear deformation theory. The displacement field assumption as follow is made firstly:

$$d = \Phi \mathbf{T} \mathbf{a} \tag{20}$$

where $\mathbf{T} = [\Phi^{\mathrm{T}}(\xi_1)\ \Phi^{\mathrm{T}}(\xi_2)\ \ldots\ \Phi^{\mathrm{T}}(\xi_{n+1})]^{-\mathrm{T}}$, is a BSWI element transform matrix, and $\mathbf{a}$ is the displacement coefficients vector in BSWI4$_3$ scaling space. For a two dimensional interpolation, the transform matrix is also the Kronecker product of two one dimensional $\mathbf{T}$. The element displacement field represented by the coefficients of wavelets is transformed from wavelet space to physical space by aid of this transform matrix.

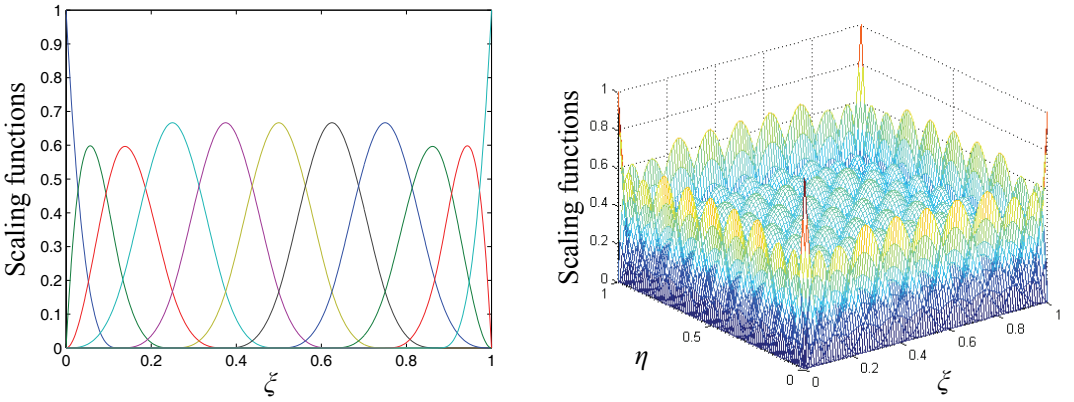

(a) One dimensional BSWI4$_3$ scaling functions (b) Two dimensional BSWI4$_3$ scaling functions

Figure 3: BSWI4$_3$ scaling functions on the interval [0, 1]

Fig. 5 shows the details of the BSWI element. Recur to the inner node of BSWI element shown in Fig. 5, the element computing area is divided as a $n \times n$ grid by interpolating functions, where $n = 2^j + m - 2$, j is the scaling parameter and $m$is the order of spline mentioned above. In this paper, BSWI4$_3$ is selected as the interpolating function. For $m = 4$ and $j = 3$, thus a 10×10 grid is obtained. The total number of nodes is 11×11.

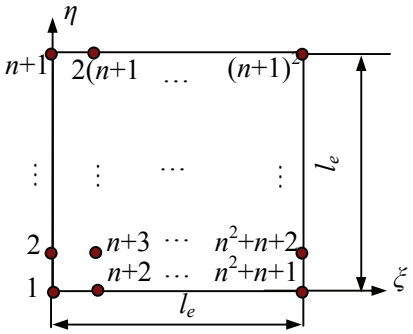

Figure 4: Illustration of the details of B-spline wavelet on the interval element.

4.1 The circular cylinder element

Substituting the corresponding Lame coefficients of circular cylinder into Eqs. (2-4) results in:

$$\boldsymbol{\varepsilon} = \mathbf{B}_{\varepsilon}\mathbf{d} = \begin{bmatrix} \frac{\partial}{\partial x} & 0 & 0 & 0 & 0 \\ 0 & \frac{1}{R}\frac{\partial}{\partial \theta} & 0 & 0 & 0 \\ \frac{1}{R}\frac{\partial}{\partial \theta} & \frac{\partial}{\partial x} & 0 & 0 & 0 \end{bmatrix} d \tag{21}$$

$$\boldsymbol{\kappa} = \mathbf{B}_{\kappa}\mathbf{d} = \begin{bmatrix} 0 & 0 & 0 & \frac{\partial}{\partial x} & 0 \\ 0 & 0 & 0 & 0 & \frac{1}{R}\frac{\partial}{\partial \theta} \\ 0 & \frac{1}{R}\frac{\partial}{\partial x} & 0 & \frac{1}{R}\frac{\partial}{\partial \theta} & \frac{\partial}{\partial x} \end{bmatrix} d \tag{22}$$

$$\boldsymbol{\gamma} = \mathbf{B}_{\gamma}\mathbf{d} = \begin{bmatrix} 0 & 0 & \frac{\partial}{\partial x} & 1 & 0 \\ 0 & -\frac{1}{R} & \frac{1}{R}\frac{\partial}{\partial \theta} & 0 & 1 \end{bmatrix} d \tag{23}$$

Substituting Eqs. (15a-c) into Eq. (13), let the variation of variational energy function equal to zero, the basic solving equation of vibration problem is obtained:

$$\left(\mathbf{K} - \omega^2 \mathbf{M}\right)\mathbf{X} = 0 \tag{24}$$

where ω is the natural frequency and $\mathbf{X}$ the mode shape of arches. The stiffness matrix $\mathbf{K}$ is defined by the summation of the three parts:

$$\mathbf{K} = \mathbf{K}^m + \mathbf{K}^b + \mathbf{K}^t \tag{25}$$

$$\mathbf{K}^m = \begin{bmatrix} \mathbf{K}^m_{11} & \mathbf{K}^m_{12} & \mathbf{K}^m_{13} & 0 & 0 \\ & \mathbf{K}^m_{22} & \mathbf{K}^m_{23} & 0 & 0 \\ & & \mathbf{K}^m_{33} & 0 & 0 \\ & \text{sym} & & 0 & 0 \\ & & & & 0 \end{bmatrix} \tag{26}$$

with

$$\mathbf{K}_{11}^{m} = D_0^m \left[R\boldsymbol{\gamma}_x^{11} \otimes \boldsymbol{\gamma}_y^{00} + (1-\nu)\boldsymbol{\Gamma}_x^{00} \otimes \boldsymbol{\gamma}_y^{11}/2R \right]$$
$$\mathbf{K}_{12}^{m} = D_0^m \left[\nu\boldsymbol{\gamma}_x^{10} \otimes \boldsymbol{\gamma}_y^{01} + (1-\nu)\boldsymbol{\gamma}_x^{00} \otimes \boldsymbol{\gamma}_y^{11}/2 \right]$$
$$\mathbf{K}_{13}^{m} = D_0^m \left[\nu\boldsymbol{\gamma}_x^{10} \otimes \boldsymbol{\gamma}_y^{00} \right]$$
$$\mathbf{K}_{22}^{m} = D_0^m \left[\boldsymbol{\gamma}_x^{00} \otimes \boldsymbol{\gamma}_y^{11}/R + (1-\nu) R\boldsymbol{\gamma}_x^{11} \otimes \boldsymbol{\gamma}_y^{00}/2 \right]$$
$$\mathbf{K}_{23}^{m} = D_0^m \left[\boldsymbol{\gamma}_x^{00} \otimes \boldsymbol{\gamma}_y^{10}/R \right] \quad \mathbf{K}_{33}^{m} = D_0^m \left[\boldsymbol{\gamma}_x^{00} \otimes \boldsymbol{\gamma}_y^{00}/R \right]$$

$$\mathbf{K}^b = \begin{bmatrix} 0 & 0 & 0 & 0 & 0 \\ & \mathbf{K}_{22}^b & 0 & \mathbf{K}_{24}^b & \mathbf{K}_{25}^b \\ & & 0 & 0 & 0 \\ & \text{sym} & & \mathbf{K}_{44}^b & \mathbf{K}_{45}^b \\ & & & & \mathbf{K}_{55}^b \end{bmatrix} \tag{27}$$

with

$$\mathbf{K}_{22}^{b} = D_0^b \left[(1-\nu)\boldsymbol{\gamma}_x^{11} \otimes \boldsymbol{\gamma}_y^{00}/2R \right]$$
$$\mathbf{K}_{24}^{b} = D_0^b \left[(1-\nu)\boldsymbol{\gamma}_x^{10} \otimes \boldsymbol{\gamma}_y^{01}/2R \right]$$
$$\mathbf{K}_{25}^{b} = D_0^b \left[(1-\nu)\boldsymbol{\gamma}_x^{11} \otimes \boldsymbol{\gamma}_y^{00}/2 \right]$$
$$\mathbf{K}_{44}^{b} = D_0^b \left[R\boldsymbol{\gamma}_x^{11} \otimes \boldsymbol{\gamma}_y^{00} + (1-\nu)\boldsymbol{\Gamma}_x^{00} \otimes \boldsymbol{\gamma}_y^{11}/2R \right]$$
$$\mathbf{K}_{45}^{b} = D_0^b \left[\nu\boldsymbol{\gamma}_x^{10} \otimes \boldsymbol{\gamma}_y^{01} + (1-\nu)\boldsymbol{\gamma}_x^{01} \otimes \boldsymbol{\gamma}_y^{10}/2 \right]$$
$$\mathbf{K}_{55}^{b} = D_0^b \left[\boldsymbol{\gamma}_x^{00} \otimes \boldsymbol{\gamma}_y^{11}/R + (1-\nu) R\boldsymbol{\gamma}_x^{11} \otimes \boldsymbol{\gamma}_y^{00}/2 \right]$$

$$\mathbf{K}^t = \begin{bmatrix} 0 & 0 & 0 & 0 & 0 \\ & \mathbf{K}_{22}^t & \mathbf{K}_{23}^t & 0 & \mathbf{K}_{25}^t \\ & & \mathbf{K}_{33}^t & \mathbf{K}_{34}^t & \mathbf{K}_{35}^t \\ & \text{sym} & & \mathbf{K}_{44}^t & 0 \\ & & & & \mathbf{K}_{55}^t \end{bmatrix} \tag{28}$$

with

$$\mathbf{K}_{22}^{t} = D_0^t \left[\boldsymbol{\gamma}_x^{00} \otimes \boldsymbol{\gamma}_y^{00}/R \right] \quad \mathbf{K}_{23}^{t} = D_0^t \left[-\boldsymbol{\gamma}_x^{00} \otimes \boldsymbol{\gamma}_y^{01}/R \right]$$
$$\mathbf{K}_{25}^{t} = D_0^t \left[-\boldsymbol{\gamma}_x^{00} \otimes \boldsymbol{\gamma}_y^{00} \right]$$
$$\mathbf{K}_{33}^{t} = D_0^t \left[R\boldsymbol{\gamma}_x^{11} \otimes \boldsymbol{\gamma}_y^{00} + \boldsymbol{\gamma}_x^{00} \otimes \boldsymbol{\Gamma}_y^{11}/R \right]$$
$$\mathbf{K}_{34}^{t} = D_0^t \left[R\boldsymbol{\gamma}_x^{10} \otimes \boldsymbol{\gamma}_y^{00} \right] \quad \mathbf{K}_{35}^{t} = D_0^t \left[\boldsymbol{\gamma}_x^{00} \otimes \boldsymbol{\gamma}_y^{10} \right]$$
$$\mathbf{K}_{44}^{t} = D_0^t \left[R\boldsymbol{\gamma}_x^{00} \otimes \boldsymbol{\gamma}_y^{00} \right] \quad \mathbf{K}_{55}^{t} = D_0^t \left[R\boldsymbol{\gamma}_x^{00} \otimes \boldsymbol{\gamma}_y^{00} \right]$$

where the details of integration matrix $\boldsymbol{\gamma}$ can be found in Appendix. The formulation of mass matrix is relatively simple:

$$\mathbf{M} = \rho R \boldsymbol{\gamma}_x^{00} \otimes \boldsymbol{\gamma}_y^{00} \begin{bmatrix} h & 0 & 0 & 0 & 0 \\ & h & 0 & 0 & 0 \\ & & h & 0 & 0 \\ & \text{sym} & & h^3/12 & 0 \\ & & & & h^3/12 \end{bmatrix} \tag{29}$$

4.2 The doubly-curved shell element

During the construction of BSWI element, the hyperbolic paraboloidal shell is regarded as a special case of doubly-curved shell. Thus, in this section, we only give the formulation of a common doubly-curved shell element. Substituting $A_1 = R_x$ and$A_2 = R_y$. into Eqs. (2-4) results in:

$$\boldsymbol{\varepsilon} = \mathbf{B}_\varepsilon \mathbf{d} = \begin{bmatrix} \frac{1}{R_x}\frac{\partial}{\partial\theta_x} & 0 & \frac{1}{R_x} & 0 & 0 \\ 0 & \frac{1}{R_y}\frac{\partial}{\partial\theta_y} & 0 & 0 & 0 \\ \frac{1}{R_y}\frac{\partial}{\partial\theta_y} & \frac{1}{R_x}\frac{\partial}{\partial\theta_x} & 0 & 0 & 0 \end{bmatrix} d \tag{30}$$

$$\boldsymbol{\kappa} = \mathbf{B}_\kappa \mathbf{d} = \begin{bmatrix} 0 & 0 & 0 & \frac{1}{R_x}\frac{\partial}{\partial\theta_x} & 0 \\ 0 & 0 & 0 & 0 & \frac{1}{R_y}\frac{\partial}{\partial\theta_y} \\ 0 & 0 & \frac{R_x+R_y}{R_xR_y} & \frac{1}{R_y}\frac{\partial}{\partial\theta_y} & \frac{1}{R_x}\frac{\partial}{\partial\theta_x} \end{bmatrix} d \tag{31}$$

$$\boldsymbol{\gamma} = \mathbf{B}_\gamma \mathbf{d} = \begin{bmatrix} -\frac{1}{R_x} & 0 & \frac{1}{R_x}\frac{\partial}{\partial\theta_x} & 1 & 0 \\ 0 & -\frac{1}{R_y} & \frac{1}{R_y}\frac{\partial}{\partial\theta_y} & 0 & 1 \end{bmatrix} d \tag{32}$$

The stiffness matrix $\mathbf{K}$ is written as the summation of the three parts as Eq. (17), denote $r_{xy} = (R_x + R_y)/R_xR_y$, then the details of $\mathbf{K}$ can be expressed as:

$$\mathbf{K}^m = \begin{bmatrix} \mathbf{K}^m_{11} & \mathbf{K}^m_{12} & \mathbf{K}^m_{13} & 0 & 0 \\ & \mathbf{K}^m_{22} & \mathbf{K}^m_{23} & 0 & 0 \\ & & \mathbf{K}^m_{33} & 0 & 0 \\ & \text{sym} & & 0 & 0 \\ & & & & 0 \end{bmatrix} \tag{33}$$

with

$$\mathbf{K}^m_{11} = D^m_0 \left[R_y \boldsymbol{\gamma}^{11}_x \otimes \boldsymbol{\gamma}^{00}_y / R_x + (1-\nu) R_x \boldsymbol{\gamma}^{00}_x \otimes \boldsymbol{\gamma}^{11}_y / 2R_y \right]$$
$$\mathbf{K}^m_{12} = D^m_0 \left[\nu \boldsymbol{\gamma}^{10}_x \otimes \boldsymbol{\gamma}^{01}_y + (1-\nu) \boldsymbol{\gamma}^{00}_x \otimes \boldsymbol{\gamma}^{11}_y / 2 \right]$$
$$\mathbf{K}^m_{13} = D^m_0 \left[R_y \boldsymbol{\gamma}^{10}_x \otimes \boldsymbol{\gamma}^{00}_y / R_x + \nu \boldsymbol{\gamma}^{10}_x \otimes \boldsymbol{\gamma}^{00}_y \right]$$
$$\mathbf{K}^m_{22} = D^m_0 \left[R_x \boldsymbol{\gamma}^{00}_x \otimes \boldsymbol{\gamma}^{11}_y / R_y + (1-\nu) R_y \boldsymbol{\gamma}^{11}_x \otimes \boldsymbol{\gamma}^{00}_y / 2R_x \right]$$
$$\mathbf{K}^m_{23} = D^m_0 \left[\nu \boldsymbol{\gamma}^{00}_x \otimes \boldsymbol{\gamma}^{10}_y + R_x \boldsymbol{\gamma}^{00}_x \otimes \boldsymbol{\gamma}^{10}_y / R_y \right]$$
$$\mathbf{K}^m_{33} = D^m_0 \left[(R_y/R_x + R_x/R_y + 2\nu) \boldsymbol{\gamma}^{00}_x \otimes \boldsymbol{\gamma}^{00}_y \right]$$

$$\mathbf{K}^b = \begin{bmatrix} 0 & 0 & 0 & 0 & 0 \\ & 0 & 0 & 0 & 0 \\ & & \mathbf{K}^b_{33} & \mathbf{K}^b_{34} & \mathbf{K}^b_{35} \\ & \text{sym} & & \mathbf{K}^b_{44} & \mathbf{K}^b_{45} \\ & & & & \mathbf{K}^b_{55} \end{bmatrix} \tag{34}$$

with

$$\mathbf{K}_{33}^{b} = R_x R_y D_0^b \left[r_{xy}^2 (1 - \nu) \boldsymbol{\gamma}_x^{00} \otimes \boldsymbol{\gamma}_y^{00} / 2 \right]$$
$$\mathbf{K}_{34}^{b} = R_x D_0^b \left[r_{xy} (1 - \nu) \boldsymbol{\gamma}_x^{00} \otimes \boldsymbol{\gamma}_y^{01} / 2 \right]$$
$$\mathbf{K}_{35}^{b} = R_y D_0^b \left[r_{xy} (1 - \nu) \boldsymbol{\gamma}_x^{01} \otimes \boldsymbol{\gamma}_y^{00} / 2 \right]$$
$$\mathbf{K}_{44}^{b} = D_0^b \left[R_y \boldsymbol{\gamma}_x^{11} \otimes \boldsymbol{\gamma}_y^{00} / R_x + R_x (1 - \nu) \boldsymbol{\gamma}_x^{00} \otimes \boldsymbol{\gamma}_y^{11} / 2R_y \right]$$
$$\mathbf{K}_{45}^{b} = D_0^b \left[\nu \boldsymbol{\gamma}_x^{10} \otimes \boldsymbol{\gamma}_y^{01} + (1 - \nu) \boldsymbol{\gamma}_x^{01} \otimes \boldsymbol{\gamma}_y^{10} / 2 \right]$$
$$\mathbf{K}_{55}^{b} = D_0^b \left[R_x \boldsymbol{\gamma}_x^{00} \otimes \boldsymbol{\gamma}_y^{11} / R_y + R_y (1 - \nu) \boldsymbol{\gamma}_x^{11} \otimes \boldsymbol{\gamma}_y^{00} / 2R_x \right]$$

$$\mathbf{K}^t = \begin{bmatrix} \mathbf{K}_{11}^t & 0 & \mathbf{K}_{13}^t & \mathbf{K}_{14}^t & 0 \\ & \mathbf{K}_{22}^t & \mathbf{K}_{23}^t & 0 & \mathbf{K}_{25}^t \\ & & \mathbf{K}_{33}^t & \mathbf{K}_{34}^t & \mathbf{K}_{35}^t \\ & \text{sym} & & \mathbf{K}_{44}^t & 0 \\ & & & & \mathbf{K}_{55}^t \end{bmatrix} \tag{35}$$

with

$$\mathbf{K}_{11}^t = D_0^t \left[R_y \boldsymbol{\gamma}_x^{00} \otimes \boldsymbol{\gamma}_y^{00} \right] \quad \mathbf{K}_{13}^t = D_0^t \left[-R_y \boldsymbol{\gamma}_x^{01} \otimes \boldsymbol{\Gamma}_y^{00} / R_x \right]$$
$$\mathbf{K}_{14}^t = D_0^t \left[-R_y \boldsymbol{\gamma}_x^{00} \otimes \boldsymbol{\gamma}_y^{00} \right] \quad \mathbf{K}_{22}^t = D_0^t \left[R_x \boldsymbol{\gamma}_x^{00} \otimes \boldsymbol{\gamma}_y^{00} \right]$$
$$\mathbf{K}_{23}^t = D_0^t \left[-R_x \boldsymbol{\gamma}_x^{00} \otimes \boldsymbol{\gamma}_y^{01} / R_y \right] \quad \mathbf{K}_{25}^t = D_0^t \left[-R_x \boldsymbol{\gamma}_x^{00} \otimes \boldsymbol{\Gamma}_y^{00} \right]$$
$$\mathbf{K}_{33}^t = D_0^t \left[R_y \boldsymbol{\gamma}_x^{11} \otimes \boldsymbol{\gamma}_y^{00} / R_x + R_x \boldsymbol{\gamma}_x^{00} \otimes \boldsymbol{\gamma}_y^{11} / R_y \right]$$
$$\mathbf{K}_{34}^t = D_0^t \left[R_y \boldsymbol{\gamma}_x^{10} \otimes \boldsymbol{\gamma}_y^{00} \right] \quad \mathbf{K}_{35}^t = D_0^t \left[R_x \boldsymbol{\gamma}_x^{00} \otimes \boldsymbol{\gamma}_y^{10} \right]$$
$$\mathbf{K}_{44}^t = D_0^t \left[R_x R_y \boldsymbol{\gamma}_x^{00} \otimes \boldsymbol{\gamma}_y^{00} \right] \quad \mathbf{K}_{55}^t = D_0^t \left[R_x R_y \boldsymbol{\gamma}_x^{00} \otimes \boldsymbol{\Gamma}_y^{00} \right]$$

The corresponding mass matrix is:

$$\mathbf{M} = \rho R_x R_y \boldsymbol{\gamma}_x^{00} \otimes \boldsymbol{\Gamma}_y^{00} \begin{bmatrix} h & 0 & 0 & 0 & 0 \\ & h & 0 & 0 & 0 \\ & & h & 0 & 0 \\ & \text{sym} & & h^3/12 & 0 \\ & & & & h^3/12 \end{bmatrix} \tag{36}$$

5 Numerical studies and comparisons

In this paper, we verify the numerical efficiency and accuracy of the present method through comparison studies. A set of numerical results are presented and supplemented by some typical mode shape illustrations. Throughout the numerical examples, the Poisson's ratio ν is assigned as 0.3, and the shear correction factors k is

selected as 0.8601 (CCCC) and 5/6 (the other boundary conditions). The analysis area is in a smooth and regular field, so only a uniform mesh is employed.

5.1 Free vibration of circular cylinder

5.1.1 Example 1: cylindrical panel

In Tab. 1 the first 10 frequencies for a CFFF boundary cylindrical panel with the physical properties R = 1m, h = 0.1m, L = 2m, θ =120°, ρ = 7800 and E = 2.1×10^{11}Pa are studied. For this problem, some referential solution has been given by Tornabene et al. using GDQ method and kinds of commercial finite element software [Tornabene, Viola and Inman (2009)]. By aid of one BSWI curved shell element, an excellent agreement between the present method and reference is achieved, and the first six mode shape obtained by BSWI is presented in Fig. 6. In addition, one BSWI element is used in the following examples if no explanation is given.

Table 1: The first10 frequencies for the cylindrical panel with CFFF boundary.

Method	Mode									
	1	2	3	4	5	6	7	8	9	10
GDQ*	58.32	90.62	146.35	230.72	263.63	278.56	339.43	430.81	489.26	511.3
Abaqus*	58.91	91.82	144.59	232.46	266.07	278.88	338.8	427.44	488.07	512.94
Ansys*	58.84	91.94	145.21	233.09	267.33	278.98	342.11	429.12	493.18	517.49
Nastran*	59.01	91.84	144.99	233.32	267.19	278.78	340.93	428.59	491.86	517.13
Straus*	58.97	91.77	145.08	232.34	266.62	278.47	341.58	427.02	491.01	514.68
Pro/Mechanica*	58.92	91.79	144.59	232.46	266.07	278.69	338.81	427.25	488.22	513.06
Present	58.97	91.95	144.56	232.76	266.94	278.95	339.21	426.58	489.02	514.27

* The solution was given by Tornabene et al. [Tornabene, Viola and Inman (2009)].

Further comparisons for BSWI cylindrical shell element with the referential solutions under different kinds of boundary conditions are presented in Tab. 2. In Tab. 2 an open spherical shell with the same physic properties as the shell investigated in Tab. 1 is studied. Three kinds of typical boundaries are selected: CFCF, FSFS and SSFF. From the comparison with the GDQ method [Tornabene, Viola and Inman (2009)], BSWI shows its accuracy in computations.

5.1.2 Example 2: closed cylindrical shell

In addition, for a comprehensive comparison, a closed cylindrical shell (θ = 360°) is investigated, too. Employing two BSWI elements, the estimations of the first 10 frequencies with the CC, SS and CS boundaries are made and presented in Tab. 3. The solution obtained by the GDQ method is also presented there [Tornabene, Viola and Inman (2009)]. The present method has a good agreement with the GDQ

Table 2: The first 10 frequencies for cylindrical panel characterized by different boundary conditions.

Frequencies (Hz)	CFCF		FSFS		SSFF	
	GDQ*	Present	GDQ*	Present	GDQ*	Present
f_1	204.87	206.20	168.18	168.15	76.18	77.27
f_2	222.97	224.88	364.40	361.99	188.14	187.56
f_3	383.58	381.38	407.33	407.76	232.26	233.83
f_4	441.11	439.00	421.67	418.85	285.37	285.03
f_5	467.98	470.82	634.29	629.86	428.84	423.76
f_6	474.78	477.74	651.69	645.32	467.63	468.60
f_7	715.01	711.55	717.89	718.07	537.52	537.91
f_8	719.14	720.63	781.15	788.76	573.73	572.80
f_9	725.44	720.97	792.79	794.05	673.55	670.28
f_{10}	736.76	738.58	806.95	807.02	731.76	724.83

* The solution was given by Tornabene et al. [Tornabene, Viola and Inman (2009)].

Table 3: The first 5 frequencies for cylindrical shell characterized by different boundary conditions.

Boundary	Method	Mode sequence number				
		1	2	3	4	5
CC	GDQ*	360.36	375.86	463.29	523.55	646.56
	Present	360.84	367.93	467.28	522.77	648.73
SS	GDQ*	331.15	348.46	440.86	508.07	596.25
	Present	328.78	347.52	438.66	507.55	600.76
CS	GDQ*	344.78	361.52	451.18	515.53	628.74
	Present	343.53	360.97	450.03	514.89	628.81

* The solution was given by Tornabene et al. [Tornabene, Viola and Inman (2009)].

method in the lower mode shapes. With the increase of mode order number, the agreement becomes weak. This phenomenon is caused by the fewer degrees of freedom is used in BSWI for estimating frequencies. It should be mentioned that the overlapped modes are neglected, and the first five different mode shapes are shown in Fig. 7.

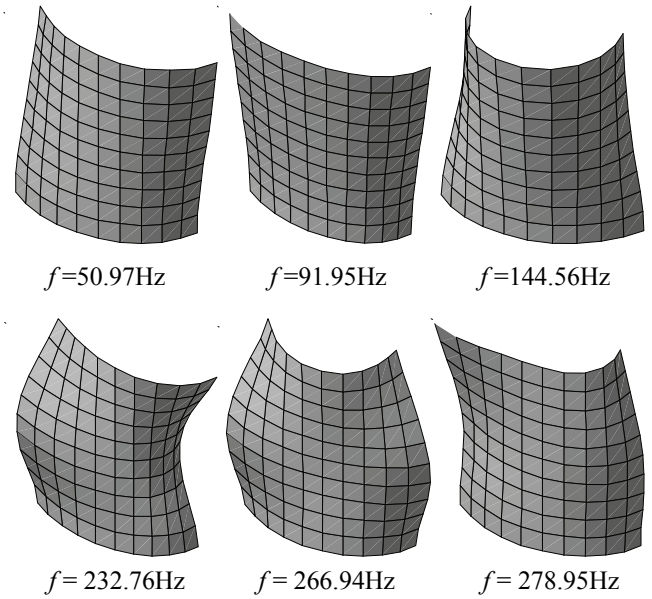

Figure 5: The first six mode shapes of CFFF cylindrical panel

Table 4: Comparison of frequency parameters $\lambda = \omega a(\rho/E)^{0.5}$ for a thin fully clamped (CCCC) shallow spherical shell.

Method	Mode sequence number							
	1	2	3	4	5	6	7	8
3-D Ritz Method*	0.57638	0.57638	0.59134	0.63038	0.64764	0.72609	0.72609	0.77493
Thin Shell Theory**	0.58099	0.58099	0.59594	0.63537	0.65422	0.73299	0.73299	0.77902
Present	0.58013	0.58028	0.59921	0.63310	0.66446	0.73952	0.73973	0.79636

* The solution was given by Liew et al. [Liew, Peng and Ng (2002)].

** The solution was given by Liew et al. [Liew and Lim (1994)].

5.2 Free vibration of doubly-curved shell

5.2.1 Example 3: thin shell

The present element is constructed based on the first order shear deformation theory, so its applicability for thin shell should be validated. Tab. 4 compares the results for a fully clamped (CCCC) thin spherical shell. The basic physical parameters are: thickness ratio $h/a = 0.01$; radius of curvature $a/R_x = 0.5$; radius ratio $R_x/R_y = 1$. The dimensionless parameter $\lambda = \omega a(\rho/E)^{0.5}$ is used to charac-

Table 5: Comparison of frequency parameters for the $\lambda = \omega ab\sqrt{\rho h/D_0^b}$ CFFF thin doubly-curved shells.

b/R_y	R_y/R_x	Method	Mode sequence number					
			1	2	3	4	5	6
0.1	0.5	Leissa*	5.0840	8.6141	23.229	30.140	31.498	57.249
		Liew**	5.0815	8.6109	23.220	30.136	31.487	57.236
		Present	5.0865	8.6021	23.217	30.138	31.480	57.247
	1.0	Leissa*	4.8282	8.6090	22.694	31.385	32.687	61.282
		Liew**	4.8259	8.6058	22.684	31.374	32.682	61.263
		Present	4.8270	8.5921	22.668	31.346	32.677	61.278
0.5	0.5	Leissa*	10.295	13.628	27.624	37.048	48.592	71.014
		Liew**	10.284	13.606	27.608	37.020	48.499	70.812
		Present	10.292	13.585	27.428	37.174	48.560	70.197
	1.0	Leissa*	9.0027	9.7809	30.476	33.998	49.237	72.253
		Liew**	9.0054	9.7612	30.404	33.943	49.024	71.849
		Present	8.8715	9.5958	29.878	33.264	48.414	70.680

* The solution was given by Leissa et al. [Leissa, Lee and Wang (1983)].
** The solution was given by Liew et al. [Liew and Lim (1996)].

Table 6: Comparison of frequency parameters $\lambda = \omega a(\rho/E)^{0.5}$ derived from the various shell theories and the present BSWI approach for moderately thick shallow spherical shells ($a/R = 0.5$).

h/a	Method	Symmetry classes and mode sequence number								
		SS1	SS2	SS3	SA1	SA2	SA3	AA1	AA2	AA3
0.1	First-order theory*	1.2106	3.1471	3.1915	1.9447	3.7149	3.8243	2.6888	4.4380	5.1226
	First-order theory**	1.2005	3.1331	1.1782	1.9314	3.7025	3.8114	2.6749	4.4281	5.1086
	3D Ritz***	1.1881	3.1075	3.1560	1.9150	3.6824	3.8029	2.6610	4.3726	5.1028
	Present	1.1863	3.0920	3.1355	1.9061	3.6666	3.7682	2.6383	4.3914	5.0852
0.2	First-order theory*	1.7638	4.3337	4.4078	2.8281	3.7653	5.1442	3.8062	4.4359	5.4412
	First-order theory**	1.7454	4.3091	4.3861	2.8046	3.7546	5.1212	3.7827	4.4243	5.4329
	3D Ritz***	1.7358	4.3197	4.3994	2.8061	3.7392	5.1465	3.8044	4.3662	5.4149
	Present	1.7265	4.3438	4.3921	2.7834	3.7333	5.0746	3.7509	4.3959	5.3920

* The solution was given by Liew and Lim [Liew and Lim (1995a)].
** The solution was given by Reddy [Reddy (1984)].
***The solution was given by Liew et al. [Liew, Peng and Ng (2002)].

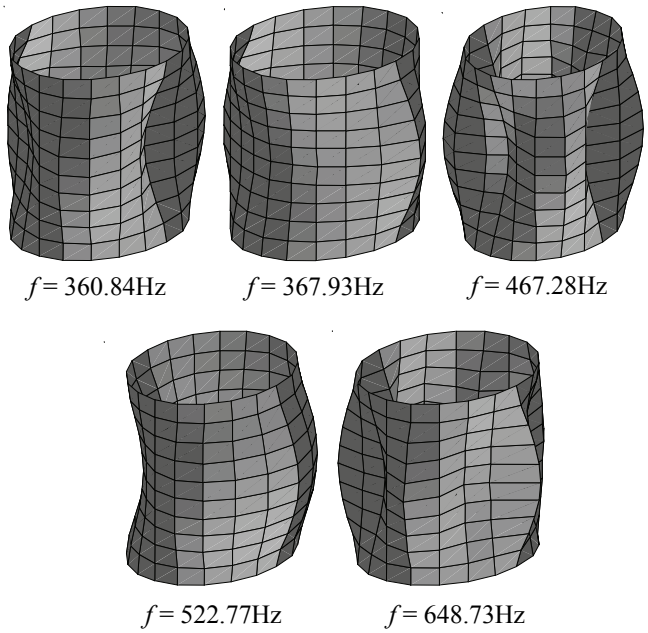

Figure 6: The first five mode shapes of CC closed cylindrical shell

terize frequency. For this problem, the relative exact solution has been obtained by Liew and Lim [Liew and Lim (1994)] using a polynomial-based Ritz method derived from thin shell theory, and another solution is given by Liew, Peng and Ng [Liew, Peng and Ng (2002)] based on the 3D-Ritz method derived from the three dimensional model and p-Ritz method. Compared with the solution obtained by 3D-Ritz method, the present solution employing one BSWI element shows a closer agreement with the solution based on thin-shell theory.

5.2.2 Example 4: moderately thick shell

Further comparisons for moderately thick shell with the predictions from the present method are presented in Tab. 5 for CFFF boundary open shell. The dimensionless frequency parameter used here is defined as $\lambda = \omega ab\sqrt{\rho h/D_0^b}$, the other properties are v = 0.3, b/h= 100.0 and a/b = 1.0. The influences to frequency caused by the variations of b/R_y and R_y/R_x are studied and compared with the frequencies obtained by Leissa et al. [Leissa, Lee and Wang (1983)] and Liew et al. [Liew and Lim (1996)]. It is clear that the solution obtained by the present method is in good agreement with their solutions in a wide parameter range, especially the thicker ones (b/R_y = 0.1).

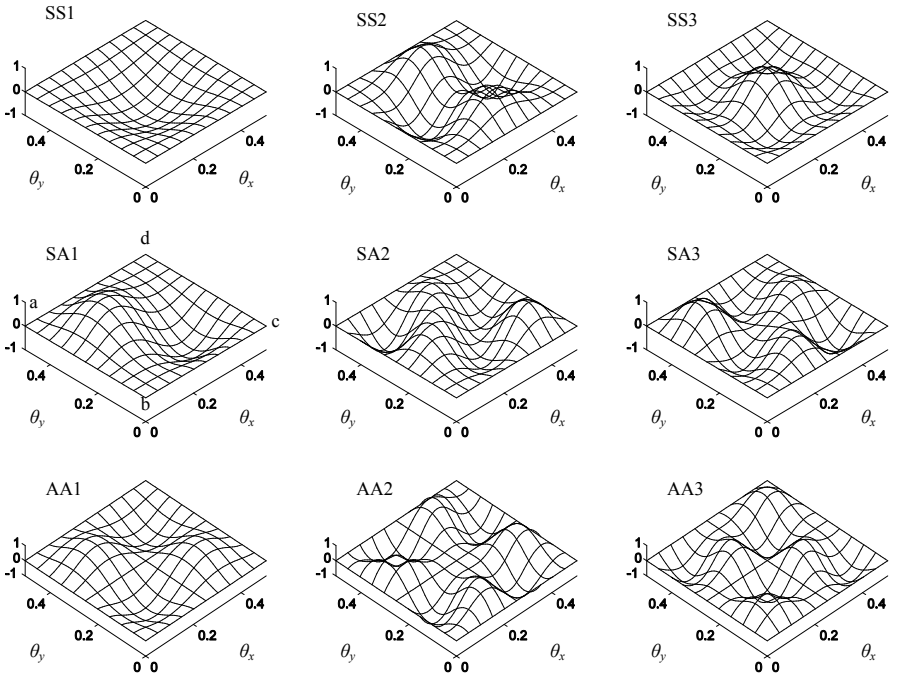

Figure 7: The mode shapes of CCCC doubly-curved shells

Another comparison is given in Tab. 6 among various theories and methods with CCCC boundary, including the first order shear deformation theory of Liew et al. [Liew and Lim (1995a)] and Reddy [Reddy (1984)]; the Ritz method based on three dimensional model [Liew, Peng and Ng (2002)]. Parameter is selected as a/R = 0.5 and $\lambda = \omega a(\rho/E)^{0.5}$. It is clear that with the increase of panel thickness, the accuracy of the three dimensional model for this problem is evident. Tab. 6 presents that the proposed method has a closer agreement with the 3D-Ritz method, thus the accuracy of the BSWI is verified. It should be mentioned that symmetry (S) and antisymmetry (A) is combined as SS, SA and AA to characterize mode shape. Because of AS modes have the same frequencies with the SA modes, they are not investigated in this paper. The corresponding mode shapes are depicted in Fig. 8. Taking the abbreviation SA1 (Fig.8) for example, S means the waveform of mode shape is symmetry in the first direction (point a to c), and A means the waveform of mode shape is symmetry in the second direction (point b to d). It should be mentioned that in SS and AA modes, the first direction is the x-axis and the second direction is the y-axis.

Table 7: Frequency parameters $\lambda = \omega a(\rho/E)^{0.5}$ for a fully clamped (CCCC) spherical shell.

a/R	*h/a*	Method	Symmetry classes and mode sequence number								
			SS1	SS2	SS3	SA1	SA2	SA3	AA1	AA2	AA3
0.1	0.01	3D Ritz*	0.17654	0.41176	0.41691	0.24755	0.51081	0.64424	0.34551	0.73883	0.74202
		Present	0.17638	0.43450	0.43987	0.24879	0.52829	0.65745	0.34687	0.74989	0.74989
	0.1	3D Ritz*	1.0008	3.1349	3.1652	1.8961	3.7368	3.7969	2.6594	4.4385	5.1590
		Present	0.9956	3.1180	3.1481	1.8859	3.7234	3.7735	2.6438	4.4376	5.1377
	0.2	3D Ritz*	1.6329	4.3730	4.4338	2.8491	3.7468	5.1950	3.8329	4.4394	5.4546
		Present	1.6202	4.3266	4.3876	2.8337	3.7272	5.1354	3.7947	4.4377	5.4346
	0.3	3D Ritz*	1.9888	4.8901	4.9619	3.2854	3.7524	5.7619	4.3433	4.4397	5.4504
		Present	1.9682	4.8136	4.8872	3.2434	3.7291	5.7487	4.2820	4.4377	5.4350
0.3	0.01	3D Ritz*	0.40471	0.50366	0.54653	0.39241	0.59206	0.70278	0.46231	0.79097	0.79798
		Present	0.40765	0.52286	0.56508	0.39393	0.60683	0.70610	0.46350	0.79581	0.79581
	0.1	3D Ritz*	1.0675	3.1267	3.1626	1.9018	3.7459	3.8020	2.6606	4.4168	5.1439
		Present	1.0635	3.1088	3.1439	1.8929	3.7035	3.7740	2.6421	4.4224	5.1495
	0.2	3D Ritz*	1.6682	4.3555	4.4223	2.8351	3.7419	5.1853	3.8236	4.4152	5.4414
		Present	1.6567	4.3461	4.4226	2.8102	3.7296	5.1154	3.7802	4.4019	5.4207
	0.3	3D Ritz*	2.0156	4.8694	4.9473	3.2577	3.7531	5.7493	4.3303	4.4099	5.4300
		Present	1.9957	4.8787	4.9350	3.2139	3.7451	5.7256	4.2618	4.4227	5.4251
0.5	0.01	3D Ritz*	0.59165	0.64815	0.77540	0.57648	0.72685	0.80683	0.63061	0.88577	0.89967
		Present	0.59921	0.66446	0.79636	0.58013	0.73952	0.81228	0.63312	0.86552	0.93432
	0.1	3D Ritz*	1.1886	3.1095	3.1579	1.9122	3.6802	3.8052	2.6625	4.3727	5.1059
		Present	1.1863	3.0902	3.1355	1.9061	3.6681	3.7682	2.6383	4.3914	5.0852
	0.2	3D Ritz*	1.7360	4.3197	4.3993	2.8062	3.7322	5.1656	3.8044	4.3662	5.4151
		Present	1.7265	4.2649	4.3921	2.7834	3.7333	5.0746	3.7509	4.3438	5.3920
	0.3	3D Ritz*	2.0678	4.8267	4.9180	3.2027	3.7533	5.7234	4.3036	4.3503	5.3902
		Present	2.0487	4.8316	4.9255	3.1592	3.7698	5.6981	4.2213	4.3921	5.4041

* The solution was given by Liew et al. [Liew, Peng and Ng (2002)].

5.2.3 Example 5: from thin to thick

In the examples mentioned above, thin shell and thick shell are studied independently. Compared with the 3D Ritz method [Liew, Peng and Ng (2002)], an investigation from thin to thick shell is given in Tab. 7. Frequency parameter is assigned as $\lambda = \omega a(\rho/E)^{0.5}$, and the boundary is selected as a fully clamped (CCCC). It can be seen that the proposed method has a good agreement with the 3D Ritz method, especially for moderately thick shells. The difference becomes bigger when the panel thickness increases. This phenomenon is due to the shell hypothesis, which neglects the stress along out-plane direction. However, it is clear that the shell element is two dimensional, thus, a great deal of computing consumption is saved to achieve a satisfying solution compared with the 3D method.

5.2.4 Example 6: hyperbolic paraboloidal shell

With the frequency parameter of $\lambda = \omega a(\rho/E)^{0.5}$ and the ratio $a/b = 1$, the estimation of BSWI for the vibration parameters for the fully clamped (CCCC) hyperbolic paraboloidal shell (R_y/R_x = -0.5) is presented in Tab. 8. The present solution is com-

Table 8: Frequency parameter of $\lambda = \omega a(\rho/E)^{0.5}$ for a CCCC moderately thick doubly-curved shallow shell with $v = 0.3$, $a/b = 1$ and different R_y/R_x.

R_y/R_x	b/R_y	h/b	Method	Symmetry classes and mode sequence number								
				SS1	SS2	SS3	SA1	SA2	SA3	AA1	AA2	AA3
-0.5	0.1	0.1	Ritz*	0.98918	3.1092	3.1383	1.8800	3.7261	3.7618	2.6346	4.4399	5.0972
			Present	0.98977	3.1019	3.1316	1.8790	3.7252	3.7508	2.6307	4.4385	5.1032
		0.2	Ritz*	1.6114	4.3090	4.3680	2.8047	3.7270	5.1124	3.7691	4.4409	5.4359
			Present	1.6171	4.2867	4.3459	2.8024	3.7265	5.0857	3.7599	4.4380	5.4345
	0.3	0.1	Ritz*	1.0207	3.1158	3.1451	1.8956	3.7208	3.7681	2.6369	4.4434	5.0973
			Present	1.0167	3.1095	3.1455	1.8966	3.7148	3.7646	2.6343	4.4305	5.1165
		0.2	Ritz*	1.6317	4.3140	4.3718	2.8143	3.7280	5.1089	3.7624	4.4518	5.4346
			Present	1.6296	4.3153	4.3783	2.8140	3.7231	5.1094	3.7723	4.4407	5.4200
0.5	0.1	0.1	Ritz*	0.99122	3.1093	3.1388	1.8805	3.7252	3.7634	2.6356	4.4395	5.0979
			Present	0.99210	3.1184	3.1484	1.8843	3.7250	3.7729	2.6438	4.4384	5.1017
		0.2	Ritz*	1.6128	4.3091	4.3685	2.8049	3.7273	5.1133	3.7707	4.4396	5.4362
			Present	1.6183	4.3275	4.3883	2.8229	3.7274	5.1213	3.7612	4.4386	5.4352
	0.3	0.1	Ritz*	1.0384	3.1167	3.1494	1.8997	3.7167	3.7788	2.6456	4.4396	5.1033
			Present	1.0334	3.1096	3.1484	1.8996	3.7144	3.7751	2.6419	4.4298	5.1216
		0.2	Ritz*	1.6437	4.3142	4.3761	2.8159	3.7309	5.1177	3.7765	4.4401	5.4369
			Present	1.6401	4.3131	4.3808	2.8036	3.7308	5.1167	3.7848	4.4310	5.4264

* The solution was given by Liew and Lim [Liew and Lim (1995a)].

pared with the solution given by Liew and Lim [Liew and Lim (1995a)] using the Ritz method based on the refined first order shear deformation theory. From Tab. 8, it is observed that the present results are in good agreement with the solutions obtained by Liew and Lim [Liew and Lim (1995a)].

6 Conclusions

A class of B-spline wavelet on interval curved shell elements are constructed in this paper. This method gives satisfactory results for free vibration analysis of structures with various curvatures, thicknesses and boundaries. The reason for getting acceptable results can be attributed to the facts that the present element is developed in generalized shell theory, which is adapted to obtain the couple of normal, tangential and rotational displacement. Another reason for getting acceptable results can be attributed to the numerical properties of B-spline wavelet on interval. By means of the numerical examples, the accuracy and efficiency of the present element are validated. It can be seen that the proposed method can obtain good results for the free vibration analysis of structures. The methodology and results presented here can help in understanding the more complicated behavior of the curved shell structures.

Acknowledgement: This work was supported by the National Natural Science Foundation of China (No. 51175401, 51035007) and FOK YING TUNG Education Foundation (No. 121052).

References

Artioli, E.; Gould, P. L.; Viola, E. (2005): A differential quadrature method solution for shear-deformable shells of revolution. *Engineering Structures*, vol. 27, pp. 1879–1892.

Atluri, S. N.; Kim, H. G.; Cho, J. Y. (1999): A critical assessment of the truly Meshless Local Petrov-Galerkin (MLPG), and Local Boundary Integral Equation (LBIE) methods. *Computational Mechanics*, vol. 24, pp. 348–372.

Atluri, S. N.; Zhu, T. (1998): A new Meshless Local Petrov-Galerkin (MLPG) approach in computational mechanics. *Computational Mechanics*, vol. 22, no. 2, pp. 117–127.

Atluri, S. N. (1985): Alternate stress and conjugate strain measures, and mixed variational formulations involving rigid rotations, for computational analyses of finitely deformed solids, with application to plates and shells-I: Theory. *Computers & Structures*, vol. 18, no. 1, pp. 93–116.

Bathe, K. J.; Iosilevich, A.; Chapelle, D. (2000): An evaluation of the MITC shell elements. *Computers & Structures*, vol. 75, pp. 1–30.

Bathe, K. J.; Lee, P. S. (1997): Finite element analysis of shell structures. *Archives of Computational Methods in Engineering*, vol. 4, no. 1, pp. 3–61.

Bathe, K. J.; Lee, P. S. (2011): Measuring the convergence behavior of shell analysis schemes. *Computers & Structures*, vol. 89, pp. 285–301.

Eucalemi, M. L.; Bathe, K. J. (1993): Higher-order MITC general shell elements. *International Journal for Numerical Methods in Engineering*, vol. 36, pp. 3729–3754.

Chao, W. C.; Reddy, J. N. (1984): Analysis of laminated composite shells using a degenerated 3-D element. *International Journal for Numerical Methods in Engineering*, vol. 20, pp. 1991–2007.

Chen, W. H.; Wu, C. W. (1995): A spline wavelets element method for frame structures vibration. *Computational Mechanics*, vol. 16, pp. 11–21.

Chen, W. H.; Wu, C. W. (1996a): Extension of spline wavelets element method to membrane vibration analysis. *Computational Mechanics*, vol.18, pp. 46–54.

Chen, W. H.; Wu, C. W. (1996b): Adaptable spline element for membrane vibration analysis. *International Journal for Numerical Methods in Engineering*, vol. 39, pp. 2457–2476.

Cowper, G. R.; Lindberg, G. M.; Olson, M. D. (1970): A shallow shell finite element of triangular shape. *International Journal of Solids and Structures*, vol. 6, pp. 1133–1156.

Goswami, J. C.; Chan, A. K.; Chui, C. K. (1995): On solving first-kind integral equations using wavelets on a bounded interval, IEEE Transactions on Antennas and Propagation, vol. 43, pp. 614-622.

Han, J. G.; Ren, W. X.; Huang, Y. (2005): A multivariable wavelet-based finite element method and its application to thick plates. *Finite Element in Analysis and Design*, vol. 41, pp. 821–833.

Han, J. G.; Ren, W. X.; Huang, Y. (2006): A spline wavelet finite-element method in structural mechanics. *International Journal for Numerical Methods in Engineering*, vol. 66, pp. 166–190.

Han, J. G.; Ren, W. X.; Huang, Y. (2007): A wavelet-based stochastic finite element method of thin plate bending. *Applied Mathematical Modelling*, vol. 31, pp. 181–193.

Huang, B. Z.; Shenoy, V. B.; Atluri, S. N. (1994): A quasi-conforming triangular laminated composite shell element based on a refined first-order theory. *Computational Mechanics*, vol. 13, no. 4, pp. 295–314.

Iura, M.; Atluri, S. N. (1992): Formulation of a membrane finite element with drilling degrees of freedom. *Computational Mechanics*, vol. 9, no. 6, 417–428.

Kang, J. H.; Leissa, A. W. (2000): Three-dimensional vibrations of thick spherical shell segments with variable thickness. *International Journal of Solids and Structures*, vol. 37, pp. 4811–4823.

Kosec, G; Sarler, B (2011): H-adaptive local radial basis function collocation meshless method. *CMC: Computers, Materials & Continua*, vol. 26, no. 3, pp. 227–254.

Kulikov, G. M.; Plotnikova, S. V. (2002): Simple and effective elements based upon Timoshenko–Mindlin shell theory. *Computer Methods in Applied Mechanics and Engineering*, vol. 191, pp. 1173–1187.

Kulikov, G. M.; Plotnikova, S. V. (2008): Finite rotation geometrically exact four-node solid-shell element with seven displacement degrees of freedom. *CMES: Computer Modeling in Engineering and Sciences,* vol. 28, no.1, pp. 15–38.

Kulikov, G. M.; Plotnikova, S. V. (2011): Finite rotation piezoelectric exact geometry solid-shell element with nine degrees of freedom per node. *CMC: Computers, Materials & Continua*, vol. 23, no. 3, pp. 233–264.

Lee, S. J.; Reddy, J. N. (2004): Vibration suppression of laminated shell structures investigated using higher order shear deformation theory. *Smart Materials and Structures*, vol. 13, pp. 1176–1194.

Leissa, A. W.; Kadi, A. S. (1971): Curvature effects on shallow shell vibrations. *Journal of Sound and Vibration*, vol. 16, pp. 173–187.

Leissa, A. W.; Lee, J. K.; Wang, A. J. (1983): Vibrations of cantilevered doubly-curved shallow shells. *International Journal of Solids and Structures*, vol. 19, pp. 411–424.

Liew, K. M.; Lim, C. W. (1994): Vibratory characteristics of cantilevered rectangular shallow shells of variable thickness. *AAIA Journal*, vol. 32, pp. 387–396.

Liew, K. M.; Lim, C. W. (1995a): A Ritz vibration analysis of doubly-curved rectangular shallow shells using a refined first-order theory. *Computer Methods in Applied Mechanics and Engineering*, vol. 127, pp. 145–162.

Liew, K. M.; Lim, C. W. (1995b): Vibratory behavior of doubly curved shallow shells of curvilinear planform. *Journal of Engineering Mechanics*, vol. 121, pp. 1277–1283.

Liew, K. M.; Lim, C. W. (1996): Vibration of doubly-curved shallow shells. *Acta Mechanica*, vol. 114, pp. 95–119.

Liew, K. M.; Lim, C. W.; Kitipornchai, S. (1997): Vibration of shallow shells: A review with bibliography. *Applied Mechanics Reviews*, vol. 50, 431–444.

Liew, K. M.; **Peng, L. X.**; **Ng, T. Y.** (2002): Three-dimensional vibration analysis of spherical shell panels subjected to deferent boundary conditions. *International Journal of Mechanical Sciences*, vol. 44, pp. 2103–2117.

Lim, C. W.; Liew, K. M. (1995): A higher order theory for vibration of shear deformable cylindrical shallow shells. *International Journal of Mechanical Sciences*, vol. 37, no. 3, pp. 277–295.

Lim, C. W.; Li, Z. R.; Wei, G. W. (2005): DSC-Ritz method for high-mode frequency analysis of thick shallow shells. *International Journal for Numerical Methods in Engineering*, vol. 62, pp. 205–232.

Nguyen-Xuan, H.; Rabczuk, T.; Bordas, S.; Debongnie, J. F. (2008): A smoothed finite element method for plate analysis. *Computer Methods in Applied Mechanics and Engineering*, vol. 197, pp. 1184–1203.

Nguyen-Xuan, H.; Bordas, S. P. A.; Nguyen-Thanh, N.; Rabczuk, T. (2008): A smoothed finite element method for shell analysis. *Computer Methods in Applied Mechanics and Engineering*, vol. 198, pp. 165–177.

Noels, L.; Radovitzky, R. (2008): A new discontinuous Galerkin method for Kirchhoff–Love shells. *Computer Methods in Applied Mechanics and Engineering,* vol. 197, pp. 2901–2929.

Olson, M. D.; Lindberg, G. M. (1971): Dynamic analysis of shallow shell with a doubly-curved triangular finite element. *Journal of Sound and Vibration*, vol. 19, pp. 299–318.

Qatu, M. S. (1992): Review of shallow shell vibration research. *The Shock and*

Vibration Digest, vol. 24, pp. 3–15.

Qatu, M. S. (1999): Theory and vibration analysis of laminated barrel thin shells. *Journal of Vibration and Control*, vol. 5, pp. 851–889.

Qatu, M. S.; Asadi, E. (2012): Vibration of doubly curved shallow shells with arbitrary boundaries. *Applied Acoustics*, vol. 73, pp. 21–27.

Reddy, J. N. (1984): Exact solutions of moderately thick laminated shells. *ASCE Journal of Engineering Mechanics*, vol. 110, pp. 794–809.

Reddy, J. N.; Arciniega, R. A. (2004): Shear deformation plate and shell theories: From Stavsky to present. *Mechanics of Advanced Materials and Structures*, vol. 11, pp. 535–582.

Sapountzakis; E. J.; Mokos, V. G. (2009): A displacement solution to transverse shear loading of composite beams by beam. *CMC: Computers, Materials, & Continua*, vol. 10, no. 1, pp. 1-40.

Tornabene, F. (2011): 2-D GDQ solution for free vibrations of anisotropic doubly-curved shells and panels of revolution. *Composite Structures*, vol. 93, pp. 1854–1876.

Tornabene, F.; Viola, E.; Inman, D. J. (2009): 2-D differential quadrature solution for vibration analysis of functionally graded conical, cylindrical shell and annular plate structures. *Journal of Sound and Vibration*, vol. 328, pp. 259-290.

Viola, E.; Tornabene, F. (2009): Free vibrations of three parameter functionally graded parabolic panels of revolution. Mechanics Research Communications, vol. 36, pp. 587–594.

Voyiadjis, G. Z.; Shi, G. Y. (1991): A refined two-dimensional theory for thick cylindrical shells. *International Journal of Solid Structure*, vol. 27, pp. 261–282.

Xiang, J. W.; Liang, M. (2011): Multiple damage detection method for beams based on multi-scale elements using hermite cubic spline wavelet. *CMES: Computer Modeling in Engineering and Sciences*, vol. 73, no. 3, pp. 267–298.

Xiang, J. W.; Long, J. Q.; Jiang, Z. S (2010): A numerical study using hermitian cubic spline wavelets for the analysis of shafts. *Proceedings of the Institution of Mechanical Engineers Part C-Journal of Mechanical Engineering Science*, vol. 224, pp. 1843–1851.

Xiang, J. W.; Matsumoto, T.; Wang, Y. X.; Jiang, Z. S. (2011): A hybrid of interval wavelets and wavelet finite element model for damage detection in structures. *CMES: Computer Modeling in Engineering & Sciences*, vol. 81, pp. 269–294.

Zhang, J. D.; Atluri, S. N. (1986): A boundary/interior element method for quasi-static and transient response analyses of shallow shells. *Computers & Structures*, vol. 24, pp. 213–223.

Zhong, Y. T.; Xiang, J. W. (2011): Construction of wavelet-based elements for static and stability analysis of elastic problems. *Acta Mechanica Solida Sinica*, vol. 24, no. 4, pp. 355–364.

Zienkiewicz, O. C.; Taylor, R. L. (2000): *The Finite Element Method, 5th ed.*, Butterworth Heinemann.

Appendix

The integration matrixes mentioned in this paper have the details as the follows:

$$\Gamma_1^{0,0} = s_{ex} \int_0^1 \mathbf{T}^{\mathrm{T}} \Phi^{\mathrm{T}} \Phi \mathbf{T} \mathrm{d}\xi \tag{A1}$$

$$\Gamma_1^{0,1} = \int_0^1 \mathbf{T}^{\mathrm{T}} \Phi^{\mathrm{T}} \frac{\mathrm{d}\Phi}{\mathrm{d}\xi} \mathbf{T} \mathrm{d}\xi \tag{A2}$$

$$\Gamma_1^{1,0} = \int_0^1 \mathbf{T}^{\mathrm{T}} \frac{\mathrm{d}\Phi^{\mathrm{T}}}{\mathrm{d}\xi} \Phi \mathbf{T} \mathrm{d}\xi \tag{A3}$$

$$\Gamma_1^{1,1} = \frac{1}{s_{ex}} \int_0^1 \mathbf{T}^{\mathrm{T}} \frac{\mathrm{d}\Phi^{\mathrm{T}}}{\mathrm{d}\xi} \frac{\mathrm{d}\Phi}{\mathrm{d}\xi} \mathbf{T} \mathrm{d}\xi \tag{A4}$$

$$\Gamma_2^{0,0} = s_{ey} \int_0^1 \mathbf{T}^{\mathrm{T}} \Phi^{\mathrm{T}} \Phi \mathbf{T} \mathrm{d}\eta \tag{A5}$$

$$\Gamma_2^{0,1} = \int_0^1 \mathbf{T}^{\mathrm{T}} \Phi^{\mathrm{T}} \frac{\mathrm{d}\Phi}{\mathrm{d}\eta} \mathbf{T} \mathrm{d}\eta \tag{A6}$$

$$\Gamma_2^{1,0} = \int_0^1 \mathbf{T}^{\mathrm{T}} \frac{\mathrm{d}\Phi^{\mathrm{T}}}{\mathrm{d}\eta} \Phi \mathbf{T} \mathrm{d}\eta \tag{A7}$$

$$\Gamma_2^{1,1} = \frac{1}{s_{ey}} \int_0^1 \mathbf{T}^{\mathrm{T}} \frac{\mathrm{d}\Phi^{\mathrm{T}}}{\mathrm{d}\eta} \frac{\mathrm{d}\Phi}{\mathrm{d}\eta} \mathbf{T} \mathrm{d}\eta \tag{A8}$$

where s_{ex} and s_{ey} are the variables with corresponding Lame coefficients in x-axis and y-axis directions, respectively (refer to Eqs (2-4)).